Future Secular Neutral Density Trends at LEO Altitudes and Their Implications for the Debris Population

Matthew K. Brown(1), Hugh G. Lewis(1), Andrew J. Kavanagh(2) and Ingrid Cnossen(2)

(1) University of Southampton, Aeronautical and Astronautical Engineering, Engineering and Physical Sciences, Tizard Building, University of Southampton, Southampton, SO17 1BJ, United Kingdom
(2) British Antarctic Survey, High Cross, Madingley Road, Cambridge, CB3 0ET, United Kingdom

ABSTRACT

Carbon dioxide (CO_2) causes global cooling in the upper atmosphere, leading to thermospheric contraction and a secular decrease in atmospheric density over time. The impact that projected greenhouse gas emissions will have upon thermospheric neutral densities through to the year 2100 have been modelled with use of the Whole Atmospheric Community Climate Model with thermosphere and ionosphere extension (WACCM-X) on the University of Southampton's high performance computing cluster, Iridis. WACCM-X numerically models the atmosphere from ground level through to the top of the thermosphere, allowing the ground emission profiles of the four Representative Concentration Pathways (RCPs) from the Intergovernmental Panel on Climate Change (IPCC) to have their effects propagated into the upper atmosphere. Secular neutral density trends dependent upon altitude have been derived for RCP8.5. The majority of currently used debris models do not include any decreasing density trend within their atmospheric component to account for greenhouse gas emissions. It has been found that under the RCP8.5 scenario, the thermospheric density at 500 km in the year 2100 will reduce by 80% when compared to the year 2000, and by 70% at 300 km. Using a simple orbital propagator which only accounts for atmospheric drag, it has been shown that orbital lifetimes will increase threefold between the year 2000 and 2100 under RCP8.5. This will have a significant impact on the debris environment.

1 INTRODUCTION

While there is well known global warming in the lower atmosphere, the opposite is true in the upper atmosphere where carbon dioxide (CO_2) contributes to global cooling. Energy is gained by CO_2 by collisional excitation, notably with atomic oxygen (O), or by absorption of infrared (IR) radiation. Energy can also be lost from excited CO_2 via the same processes, either collisions with other molecules or IR radiation at a wavelength of 15 μm. In the lower atmosphere this IR radiation is quickly reabsorbed leading to warming, but in the much thinner upper atmosphere, the radiation is lost to space or the lower atmosphere and leads to cooling. In the thermosphere, this cooling results in thermospheric contraction and a decrease in atmospheric density at any given altitude. Solar activity also affects thermospheric densities, with the roughly 11-year solar cycle seeing variation in densities of an order of magnitude. There are also smaller, daily variations in solar activity.

The secular decrease in thermospheric density caused by a secular increase in CO_2 concentration is of particular note for all objects orbiting in Low Earth Orbit (LEO). With decreasing density, the amount of atmospheric drag an orbiting object experience also reduces. This paper will focus primarily on objects with apogees below 500 km where drag is a dominant perturbing force and the effect of a secular density trend is significant. The smaller drag force leads to a smaller decrease in semi-major axis over a given time, and hence a longer orbital lifetime. Observations of changes in the semi-major axis of LEO objects have historically been used to measure density trends [1–5], with these summarized at an altitude of 400 km in Table 1. All of these studies have found the historical secular trend to be negative, with values ranging from -2.5% to -7.2% under low solar activity. The magnitude of the trend decreases with increasing levels of solar activity.

This paper will focus primarily on objects with perigees below 500 km where drag is a dominant perturbing force and so the effect of a secular density trend is significant. While this density trend and its associated increase in orbital lifetimes is advantageous for active missions (for example, in less fuel being required for orbital maintenance), it has been predicted to have a negative impact on the debris environment as atmospheric drag is the only natural way objects are removed from LEO orbit. Debris models often make predictions up to 100 years into the future and secular density trends will have a significant cumulative effect over this timespan. Reference [4] ran the Debris Analysis and Monitoring Architecture for the Geosynchronous Environment (DAMAGE) debris model

with a secular density trend which was derived from historic satellite orbit data used in [6][7]. This study showed that with a future secular density trend of around -7.2 % / decade, there is a reduction in the effectiveness of Active Debris Removal (ADR) and debris mitigation measures. Within the mitigation-only scenario, the density trend increases the LEO population growth rate by 74% over 70 years (2010 - 2080).

Table 1. Summary of historic trends at 400 km altitude.

Paper	Model or Observation	Solar activity level	Change per decade
Roble and Dickinson 1989 [8]	Model (Global Mean Model)	Low to Average	~ -3%
Rishbeth and Roble 1992 [9]	Model (TI-GCM)	Low to Average	~ -2%
Keating 2000 [1]	Observation	Low	-5.0 ± 1.4%
Marcos 2005 [2]	Observation	Average	-1.7 ± 2.4%
Qian 2006 [10]	Model (TIME-GCM)	Low	-2.5%
Emmert 2008 [3]	Observation	Low	-5.5 ± 1.4%
Saunders 2011 [11]	Observation	Low to Average	-7.2%
Emmert 2015 [5]	Observation	All	-3.0 ± 1.0%
Solomon 2015 [12]	Model (TIME-GCM)	Low	-4.9%
Solomon 2018 [13]	Model (WACCM-X)	Low	-3.9%
Solomon 2019 [14]	Model (WACCM-X)	High	-1.7%

In the Intergovernmental Panel on Climate Change (IPCC)'s Fifth Assessment Report (AR5), four Representative Concentration Pathways (RCPs) were published [15]. These are entitled RCP3, RCP4.5, RCP6.0 and RCP8.5, where the posterior number refers to the radiative forcing in 2100 in W/m^2 for each scenario. While these are not meant to be a prediction of the future, they provide a limited number of baseline scenarios from which modelling can be performed and results across studies compared. With data provided for the year 2000 through to 2100, trends can be calculated and then applied to a debris model as well as being able to be related to ground based climate change studies.

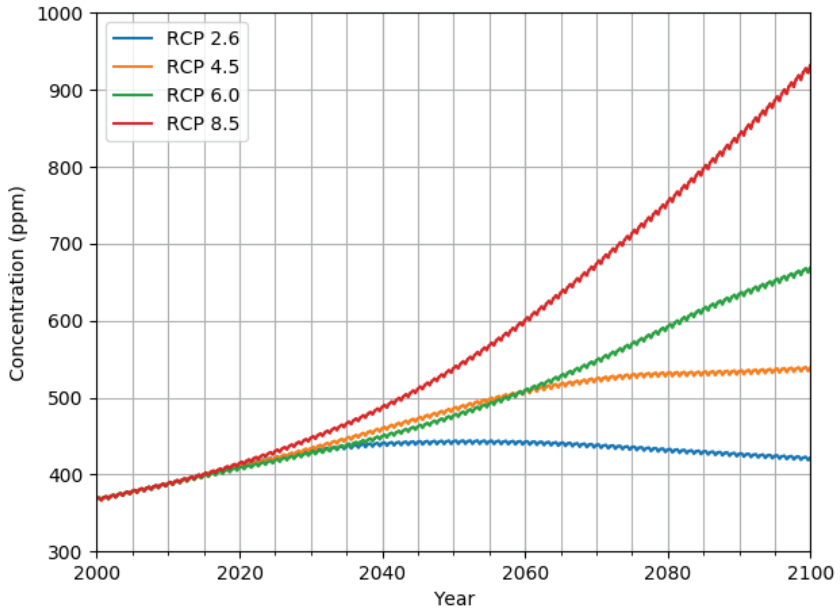

Fig. 1. Carbon dioxide concentration under the four IPCC RCP scenarios.

Table 2. Carbon dioxide concentration scales relative to 2000 levels for the four RCP scenarios.

	2005	2015	2025	2035	2045	2055	2065	2075	2085	2095
RCP3	1.028	1.087	1.147	1.185	1.199	1.201	1.194	1.179	1.164	1.149
RCP4.5	1.028	1.085	1.147	1.215	1.286	1.353	1.405	1.436	1.444	1.454
RCP6.0	1.028	1.084	1.137	1.192	1.258	1.339	1.437	1.551	1.673	1.772
RCP8.5	1.028	1.090	1.171	1.270	1.393	1.548	1.735	1.946	2.174	2.415

2 ATMOSPHERIC MODEL - WACCM-X

The National Centre for Atmospheric Research (NCAR)'s Community Earth System Model (CESM) allows for simulation of the whole, coupled Earth climate, using separate modules for each major system. In this paper the Whole Atmosphere Community Climate Model - eXtended (WACCM-X) module is used [16]. This numerically models the atmosphere from ground level through to $4x10^{-10}$ hPa (around 500 to 600 km at CO_2 levels from the year 2000 and with low solar activity). The model has a resolution of 1.9° in latitude and 2.5° in longitude (a 144 x 96 grid), with 81 vertical pressure levels and a resolution of one-quarter scale height above 1 hPa. For a full description of the chemistry and radiative transfer within WACCM-X, see [16]. For this paper, CESM 1.2.2 was run on the University of Southampton's computing cluster, Iridis 4.

WACCM-X uses initial files containing all the data needed to start a simulation. For simulations of the future, the model is usually run forwards in time. A snapshot can be taken at a certain time to act as the initial conditions for another simulation. However, this would prove infeasible due to the runtime required for simulations of 100 years within WACCM-X. Instead initial files were created by scaling the CO_2 and carbon monoxide (CO) concentrations at every pressure level in the default year 2000 files. Originally, there was an attempt to input only ground based emissions and allow them to propagate up into the thermospheric layers to create a more stable initial file set. However, spin up times approached over 10 model years, so this method would prove unsuitable with the allowed computing allocation upon Iridis. However, this long simulation alongside other publicly available, default files for historic years showed that simply scaling the CO_2 and CO concentration at each pressure level by the ground level concentration in the wanted year compared to 2000 (year of the initial file being edited) provided an initial file which span up a lot faster. The ground level CO_2 concentrations are shown in Fig. 1**.**, and these are divided by the 2000 CO_2 concentration to obtain the scales given in Table 2.

Only the concentrations of CO_2 and CO are scaled within the initial files as this accounts for over 99.7% of carbon within the thermosphere. Both have to be scaled as they react in chemical equilibrium but more CO exists than CO_2 at higher altitudes. One problem with this method is methane (CH_4) and other minor constituents are not scaled during the creation of the initial files, and instead are left to stabilize as the model runs. The minor constituents do not scale as simply as CO_2 and CO and in the pursuit of getting the model producing data, it was decided to ignore these as they have a small effect on thermospheric density when compared to the expected interannual variability, as Section 2.2 will show.

Nitric Oxide (NO) also plays a significant role in thermospheric cooling during solar maximum [17], and is increased by the anthropogenic emission of the greenhouse gas Nitrous Oxide (N_2O). However, the large amount of Nitrogen (N_2) in the lower atmosphere acts as a reservoir, keeping NO in the thermosphere at a relatively stable level. To remove the effects of solar activity (and therefore also NO) on cooling and the secular density trend, the F10.7 and Kp indices were held fixed at 70 and 0.33 respectively in all simulations. The impact of solar activity on the historic trend was investigated in [14] where it was shown the secular trend in temperature in the thermosphere decreases under high solar activity from 3 K per decade to 2 K per decade. Its impact on future secular trends will be investigated in future work.

The Earth's magnetic field also changes over time, affecting the ionosphere and in turn the thermosphere [18]. Reference [18] found that for 1908 to 2008, the historic changes in the magnetic field contribute to cooling at 300 km, however, the increasing CO_2 dominates the thermospheric cooling. The impact of the changing magnetic field will therefore not be considered in this paper. The magnetic field within WACCM-X (International Geomagnetic Reference Field (IGRF-12) [19]) is held fixed at the year 2000 level.

2.1 Converting Fixed Atmospheric Levels to Any Geometric Altitude

WACCM-X only outputs data at 81 discreet pressure levels, which vary in altitude as the atmosphere expands and contracts. The model also outputs a geopotential altitude, h, which relates to each of these levels. These can be converted into geometric altitude, z, via the relation:

$$z = h\left(1 - \frac{h}{r_E}\right) \tag{1}$$

where r_E is the radius of Earth. This geometric altitude is then directly related to the orbiting altitude and is referred to solely as altitude through the rest of the paper.

1-D monotonic cubic interpolation is performed to obtain densities and temperatures between the levels. For simulations at year 2000 CO_2 concentrations, the maximum altitude of WACCM-X is around 600 km. However, under double current CO_2 concentrations, the maximum altitude contracts down to around 300 km. Extrapolation therefore has to be used to reach LEO altitudes and calculate future trends. It was found that the function that best fit the densities above 150 km for all cases was given by

$$\rho(z) = az^b \log(z + c) + d \tag{2}$$

where ρ is density and a, b, c & d are coefficients fit to the daily global mean density with non-linear least squares to obtain a new function for each day. A better method for extrapolation is currently being searched for as the model cannot be extended to greater heights. Temperature extrapolation is much simpler as it tends towards a fixed temperature and so can just be held constant at the maximum modelled temperature. Extrapolated density and temperature profiles are shown in Fig. 2.

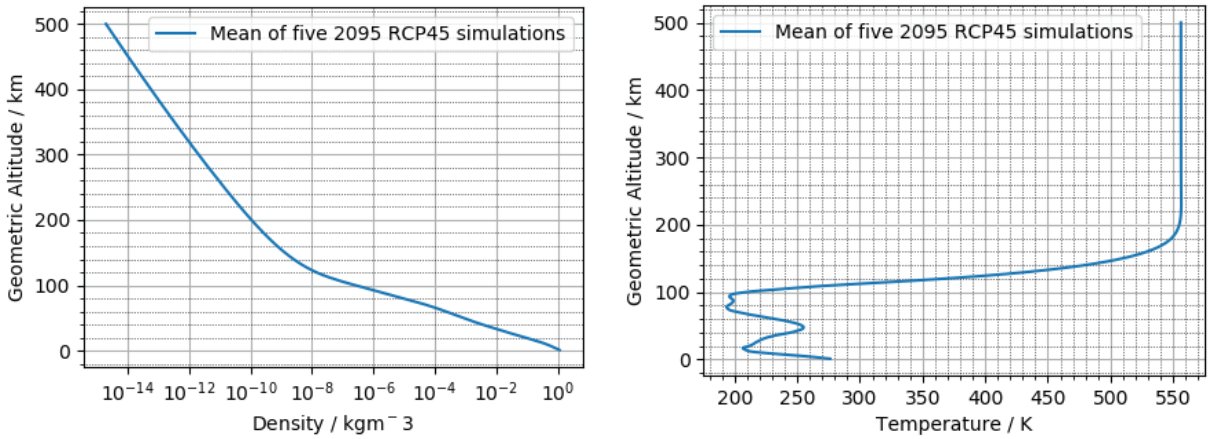

Fig. 2 WACCM-X density and temperature profiles, where extrapolation has occurred above 300 km.

2.2 Interannual Variability of Temperature and Density within WACCM-X

Reference [13] found considerable interannual variation within WACCM-X. Following their lead, an investigation was made into this variability of temperature and density to better understand the uncertainty within the model. CESM was initialized with 2095 CO_2 RCP4.5 levels, and all inputs were set as cyclical, repeating the year 2095, such that the end of one run is used as the start of the next. The year 2095 was simulated five times under these conditions, with the results being plotted in Fig. 3 and Fig. 4. Reference [13] used the mean of a five-year ensemble within their study to account for this variability, however this is not possible within our study due to the number of simulations which need to be run.

Further investigation into the 2095e value needs to be undertaken as there is a possibility that as the minor constituents equilibrate after the large increase in atmospheric carbon, a major unforeseen change occurs within the atmosphere. Reference [13] saw interannual variation in 5 year ensembles of around 2.5 K whereas we see 6 K (or 4 K discounting 2095e). The relative temperature difference only approaches a maximum of 0.65% for 2095e but this relates to a relative density difference of 5% from our ensemble mean.

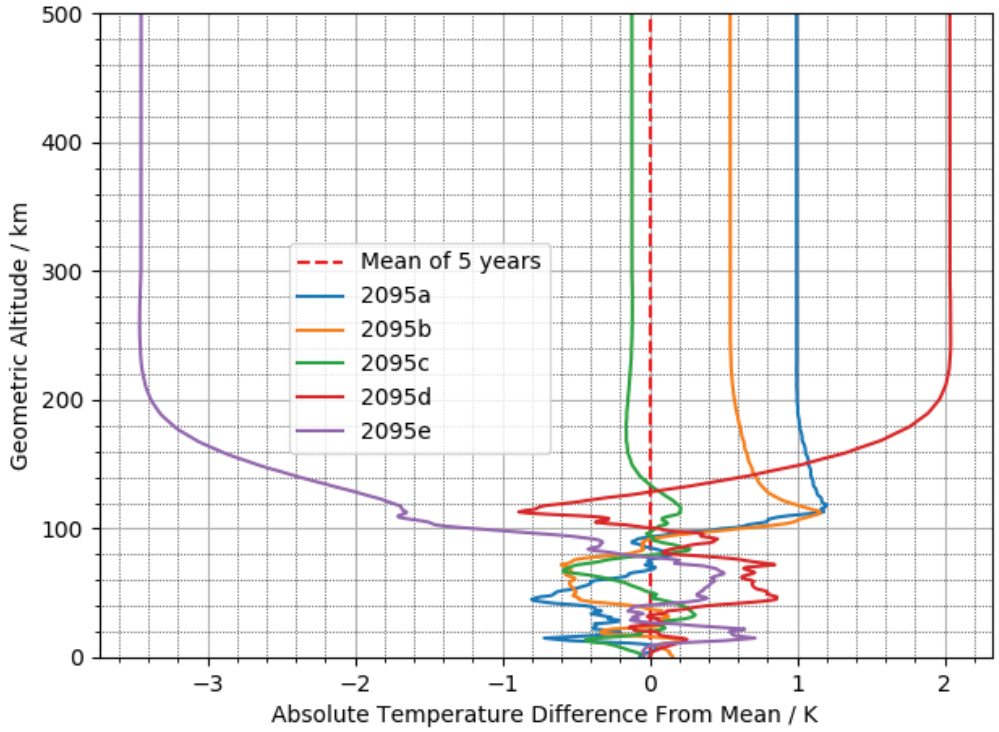

Fig. 3. Interannual absolute temperature difference from the mean of the five simulations of the year 2095 under RCP4.5. The mean profile is shown in Fig. 2.

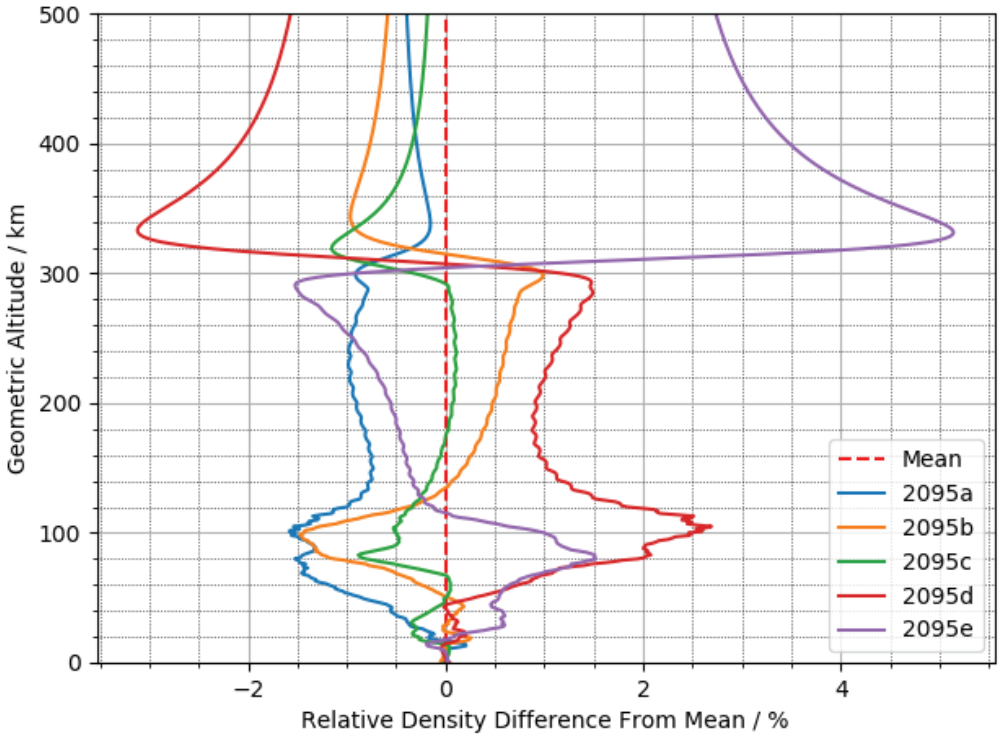

Fig. 4. Interannual relative density difference from the mean of the five simulations of the year 2095 under RCP4.5. The mean profile is shown in Fig. 2.

3 FUTURE DENSITY TREND CALCULATION AND APPLICATION

The atmosphere under RCP8.5 has been simulated with WACCM-X for the years 2015, 2045, 2055, 2065, 2075 and 2095, each with initial files scaled as specified earlier. Data for each year was then converted from pressure levels to geometric altitudes, and interpolated and extrapolated as required. To remove both geographic and seasonal variation, the model data is averaged over all latitudes and longitudes, as well as averaged over each whole year to give a "global mean annual mean" for each year.

The relative difference between each successive yearly global mean annual mean pair was calculated, and then divided by the number of decades between the two modelled years in order to obtain the secular trends in % per decade. These calculated trends are shown in Fig. 5. The historic density trend between 1972 and 2005 calculated using a similar method within [13] is also included.

By attributing the trends to the midpoint of the two years they are calculated from, a yearly trend (in % per year) for any individual year can then be found via linear interpolation. These are cumulatively multiplied together from the year 2000 to obtain a cumulative atmospheric density reduction as shown in Fig. 6. The yearly trend for the period 2000-2030 is held equal to the historic 1972-2005 level, and the 2085-2100 is held equal to the calculated 2075-2095 trend. This assumption will be improved upon with further simulated years in the future.

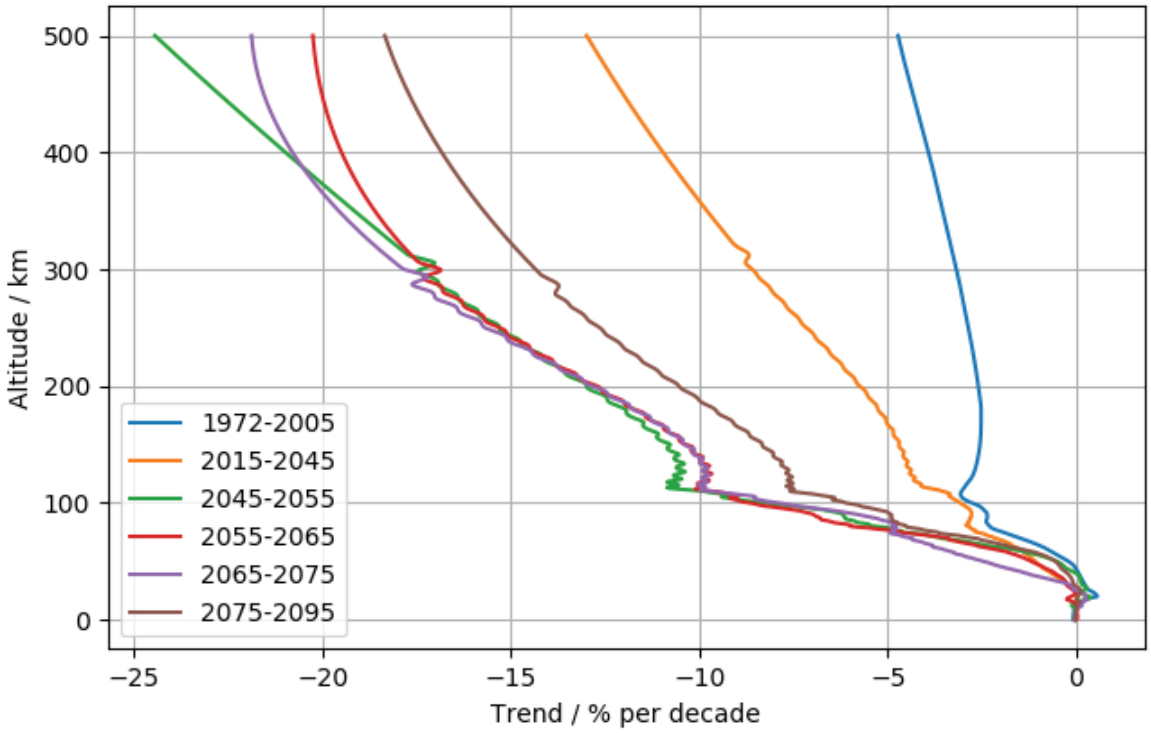

Fig. 5. Trends in thermospheric density through to 2095 under RCP8.5 due to CO_2 emissions only. Data for 1972-2005 is taken from [13].

The cumulative density reduction can be used as a scaling factor for an empirical atmospheric model in order to obtain densities at any given future time up to 2100 which includes the secular trend. The Naval Research Lab's Mass Spectrometer and Incoherent Scatter Radar Exosphere - 2000 (NRLMSISE-00) atmospheric model has been chosen here because the historical data used to calibrate the model matches well with the years used to calculate the historic trend in [20]. It should again be noted that all trends here have been calculated only under low solar activity so the scaled density model should only be used under low solar activity too.

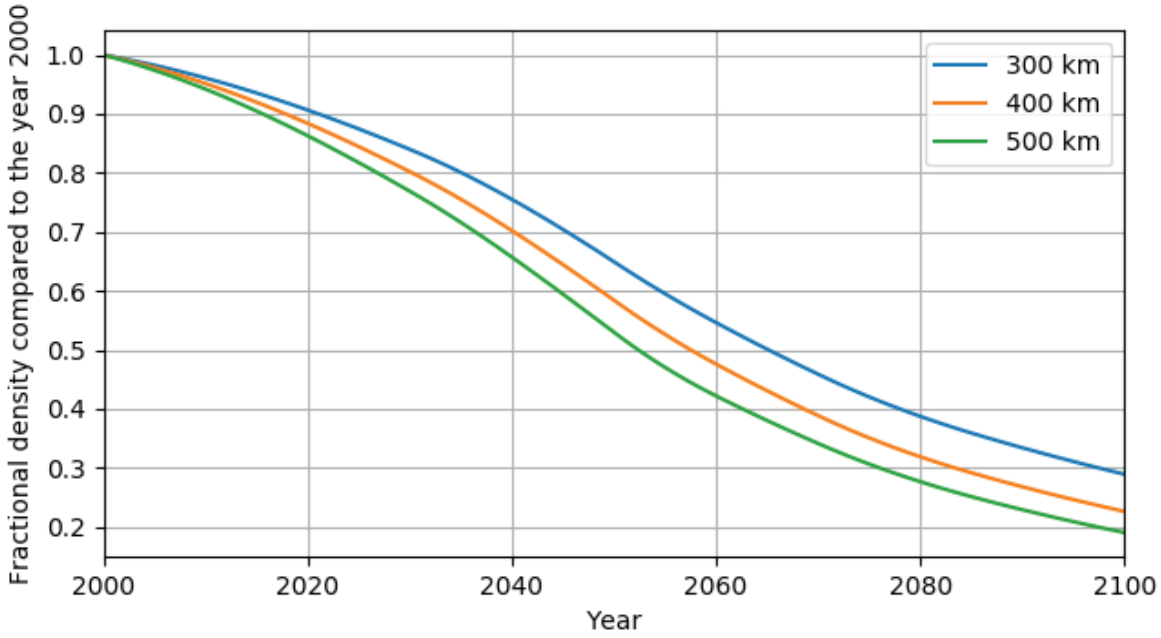

Fig. 6. Atmospheric density in the RCP8.5 scenario referenced against the year 2000.

4 IMPACT ON ORBITAL LIFETIMES

A simple orbital propagator which had drag as the only perturbing force has been used to calculate lifetimes for some example objects, with results summarized in Table 3. Each object was propagated from the same initial orbit with no trend applied (year 2000) and with the cumulative effect of the RCP8.5 trend applied for the year 2050 and 2100. NRLMSISE-00 has been used as the base atmospheric model to which the cumulative trend is applied as the years of data used to calibrate this atmospheric model match well with the years used by [13] to calculate the historic, base trend. Applying the cumulative trend calculated via WACCM-X to an empirical model fills the time gaps in density data from WACCM-X and can be applied as a simple scaling factor to other empirical models. This avoids having to download the large datasets created by WACCM-X.

Table 3. Calculated orbital lifetimes for various LEO objects with the CO_2 trend applied. The coefficient of drag was held at 2.0 for each object, except for Humanity Star, which was set as 0.66.

	Test Object	**ISS**	**RemoveDebris (sail deployed)**	**Starlink-60**	**MicroSat-R Debris**	**Humanity Star**
NORAD ID	-	25544	43510	44273	44203	43168
Perigee and apogee / km	200 × 900	407 × 427	390 × 403	420 × 446	264 × 523	288 × 533
Area/mass ratio / m^2/kg	0.00785	0.00337	0.250	0.0176	0.00530	0.0785
Lifetime in year 2000 /days	389.7	1695.2	15.7	483.4	334.3	63.4
Lifetime in year 2050 / days	556.9	2639.8	25.8	796.3	506.1	96.2
Lifetime in year 2100 / days	1113.8	5371.6	63.3	1848.8	1075.9	218.5

Orbital lifetimes increase as the thermospheric density decreases due to CO_2 emissions. Under RCP8.5, orbital lifetimes are between 1.43 (test object) and 1.65 (Starlink-60) times longer in the year 2050 than in 2000. Atmospheric densities reduce even further by the year 2100, leading to lifetimes between 2.86 (test object) and 4.03 (RemoveDebris) times longer in 2100 than the year 2000.

It is worth noting that Post Mission Disposal (PMD) orbits with perigees much lower than their apogees have increases in lifetime roughly equal to one over the fractional cumulative density at their perigee. For example, Humanity Star experiences a 3.45 times longer lifetime in 2100 compared to 2000, equivalent to $1/0.29$ where 0.29 is the fractional cumulative density in 2100 at 300km. This will have a severe impact on the future effectiveness of debris mitigation via the use of PMD orbits, with perigees having to be lowered further to achieve similar de-orbit times to their current rate.

Orbits with a smaller eccentricity have their lifetimes increased by a greater amount as much less time is spent at lower altitudes where the density and hence drag is relatively larger. All objects within the LEO debris environment will experience longer orbital lifetimes, reducing the effectiveness of the atmosphere as a sink for debris. Reference [4] has already shown that the effectiveness of both ADR and PMD are reduced under an atmospheric density trend of -7.2% / decade, with the LEO debris population growing by 74% extra over the period 2010-2080.

5 FAST DEBRIS MODEL - FUTURE WORK

The trends under RCP8.5 are much higher than those in [4], and so it is predicted the LEO debris population would increase even further. We aim to investigate this as well as more quickly searching the parameter space to find interesting scenarios which can be studied in further detail by a numerical debris model such as DAMAGE [6]. Therefore a relatively simple, fast debris model based on the STochastic Analog Tool (STAT) [21] is being developed. This new model is being tuned for quick investigation of the debris environment in LEO under varying density trends.

Objects in the ESA Database and Information System Characterising Objects in Space (DISCOS) reference environment are binned by semi-major axis, eccentricity, inclination and mass (a, e, i, m respectively). At each model step, objects from the DISCOS launch data can also be added into these bins to simulate launches. Representative objects which take the central values of each bin are analytically propagated at each step by calculating the change in a & e due to drag only. The propagated bin then overlaps multiple bins, and so the number of objects within the propagated bin is split by the ratio of the bin within the original bin structure. Objects can be propagated out of the bottom of the binned range, simulating deorbit via drag.

To simulate collisions, an Intrinsic Collision Probability (ICP) is calculated for each sub-bin (a, e, i) pairing, again using representative objects at the centre of each bin. This is used to generate a representative collision probability for each (a, e, i, m) pairing by multiplying by the combined cross-sectional area, $\pi(r + R)^2$ where r and R are the radii of the representative object in either bin. This representative collision probability is the same at each time step so is calculated at the start of the model simulation, stored, and called at each step. The mean number of collisions between the objects in the two bins within a time step is found by multiplying the representative collision probability by the number of objects in each bin and the size of the time step. The mean number of collisions is used within a Poisson distribution and tested against a random number in a uniform distribution between 0 and 1 in order to give a random, integer number of collisions deemed to have occurred between the two bins during the current time step.

While the ICP in STAT was found by the Wetherill algorithm [22], the new debris model uses the Bottke corrected Greenberg algorithm [23][24]. This decision was made as the calculated ICPs more closely match other more detailed algorithms but only require the a, e & i of the two objects of interest. This algorithm only holds under the assumption that the argument of perigee and the right ascension of the ascending node are uniformly distributed between 0 and 2π for both objects. This holds in our case as orbital perturbations on objects in LEO over the long time steps of the model will result in the uniform distribution required. However, it should be noted, this assumption does not hold when investigating large constellations due to multiple satellites sharing the same orbit, breaking the assumption of uniformity due to there being larger populations at certain values of ascending node. The average probability of a collision between the representative objects of the two bins is then obtained by integrating over all of the possible orbital geometries which could result in a collision.

Work is taking place to add further features before making the first investigations with the model.

6 CONCLUSION

Carbon dioxide emissions are causing cooling of the upper atmosphere, leading to thermospheric contraction and the decrease in atmospheric density at LEO altitudes. This trend has historically been observed and modelled, and in this paper has been modelled into the future for the first time, specifically under a high emission RCP8.5 scenario. The model used was WACCM-X under low solar activity conditions and a magnetic field fixed to that of the year 2000, so only the impact of CO_2 emissions on thermospheric density trends was studied. It has been found the trend in thermospheric density can reach a maximum of -24% / decade in 2050 at an altitude of 500 km, with full detail given in Fig. 5. The simulated trends are multiplied together in order to see the cumulative impact on thermospheric densities in Fig. 6. It has been found that the thermospheric density will reduce by 80% at an altitude of 500 km in the year 2100 compared to the year 2000, and by 70% at 300 km.

With the use of a simple orbital propagator, orbital lifetimes have been shown to drastically increase in the future under the RCP8.5 scenario. RemoveDebris, with its dragsail deployed, would take four times longer to de-orbit in the year 2100 compared to the year 2000. PMD orbits are also impacted but to a slightly lesser extent, with them taking one over the cumulative density reduction at their perigee altitude. This will have significant impacts on debris mitigation efforts within the LEO environment. PMD orbits will require lower perigees than currently used to achieve the same deorbit times. Work is ongoing on a fast debris model to evaluate the impact of these density trends on the LEO debris environment.

Finally, it should be noted this study has currently only looked at the high emission RCP8.5 scenario. The other scenarios will be looked at next. All studies of the historic environment show a negative density trend due to CO_2 emissions, and CO_2 concentrations increase even under the low emission scenario RCP2.6. There will be an impact on the debris environment due to lower thermospheric densities in the future, even under a low greenhouse gas emission scenario.

7 ACKNOWLEDGEMENTS

The authors acknowledge the use of the IRIDIS High Performance Computing Facility, and associated support services at the University of Southampton, in the completion of this work.

This work was supported by the Natural Environment Research Council [grant number NE/L002531/1].

8 REFERENCES

[1] G. M. Keating, R. H. Tolson, and M. S. Bradford, “Evidence of long term global decline in the Earth’s thermospheric densities apparently related to anthropogenic effects,” *Geophys. Res. Lett.*, vol. 27, no. 10, pp. 1523–1526, 2000.

[2] F. A. Marcos, J. O. Wise, M. J. Kendra, N. J. Grossbard, and B. R. Bowman, “Detection of a long-term decrease in thermospheric neutral density,” *Geophys. Res. Lett.*, vol. 32, no. 4, pp. 1–4, 2005.

[3] J. T. Emmert, J. M. Picone, and R. R. Meier, “Thermospheric global average density trends, 1967-2007, derived from orbits of 5000 near-Earth objects,” *Geophys. Res. Lett.*, vol. 35, no. 5, pp. 1–5, 2008.

[4] H. G. Lewis, A. Saunders, G. G. Swinerd, and R. J. Newland, “Effect of thermospheric contraction on remediation of the near-Earth space debris environment,” *J. Geophys. Res. Sp. Phys.*, vol. 116, no. 8, pp. 1–10, 2011.

[5] J. T. Emmert, “Altitude and solar activity dependence of 1967–2005 thermospheric density trends derived from orbital drag,” *J. Geophys. Res. Sp. Phys.*, pp. 2940–2950, 2015.

[6] H. G. Lewis, G. G. Swinerd, N. Williams, and G. Gittins, “DAMAGE: A dedicated GEO debris model framework,” *Eur. Sp. Agency, (Special Publ. ESA SP*, vol. 1, no. 473, pp. 373–378, 2001.

[7] J. T. Emmert, J. M. Picone, J. L. Lean, and S. H. Knowles, “Global change in the thermosphere: Compelling evidence of a secular decrease in density,” *J. Geophys. Res. Sp. Phys.*, vol. 109, no. A2, pp. 1–12, 2004.

[8] R. G. Roble and R. E. Dickinson, “How will changes in carbon dioxide and methane modify the mean structure of the mesosphere and thermosphere?,” *Geophys. Res. Lett.*, vol. 16, no. 12, pp. 1441–1444, 1989.

[9] H. Rishbeth and R. G. Roble, "Cooling of the upper atmosphere by enhanced greenhouse gases - modelling of thermospheric and ionospheric effects," *Planet. Space Sci.*, vol. 40, no. 7, pp. 1011–1026, 1992.

[10] L. Qian, R. G. Roble, S. C. Solomon, and T. J. Kane, "Calculated and observed climate change in the thermosphere, and a prediction for solar cycle 24," *Geophys. Res. Lett.*, vol. 33, no. 23, pp. 1–5, 2006.

[11] A. Saunders, H. G. Lewis, and G. G. Swinerd, "Further evidence of long-term thermospheric density change using a new method of satellite ballistic coefficient estimation," *J. Geophys. Res. Sp. Phys.*, vol. 116, no. 10, pp. 1–15, 2011.

[12] S. C. Solomon, L. Qian, and R. G. Roble, "New 3-D simulations of climate change in the thermosphere," *J. Geophys. Res. Sp. Phys.*, vol. 120, no. 3, pp. 2183–2193, 2015.

[13] S. C. Solomon, H. L. Liu, D. R. Marsh, J. M. McInerney, L. Qian, and F. M. Vitt, "Whole atmosphere simulation of anthropogenic climate change," *Geophys. Res. Lett.*, vol. 45, no. 3, pp. 1567–1576, 2018.

[14] S. C. Solomon, H. L. Liu, and D. R. Marsh, "Whole Atmosphere Climate Change : Dependence on Solar Activity," *J. Geophys. Res. Sp. Phys.*, pp. 3799–3809, 2019.

[15] IPCC, *Climate Change 2014 Synthesis Report*. 2014.

[16] H. L. Liu *et al.*, "Thermosphere extension of the Whole Atmosphere Community Climate Model," *J. Geophys. Res. Sp. Phys.*, vol. 115, no. 12, pp. 1–21, 2010.

[17] M. G. Mlynczak, L. A. Hunt, J. M. Russell, B. T. Marshall, C. J. Mertens, and R. E. Thompson, "The global infrared energy budget of the thermosphere from 1947 to 2016 and implications for solar variability," *Geophys. Res. Lett.*, vol. 43, no. 23, pp. 11,934-11,940, 2016.

[18] I. Cnossen, "The importance of geomagnetic field changes versus rising CO2 levels for long-term change in the upper atmosphere," *J. Sp. Weather Sp. Clim.*, vol. 4, p. 8, 2014.

[19] E. Thébault, C. C. Finlay, and C. D. Beggan, "International geomagnetic reference field: The 12th generation international geomagnetic reference field - The twelfth generation," *Earth, Planets Sp.*, vol. 67, no. 1, 2015.

[20] J. M. Picone, A. E. Hedin, D. P. Drob, and A. C. Aikin, "NRLMSISE-00 empirical model of the atmosphere: Statistical comparisons and scientific issues," *J. Geophys. Res. Sp. Phys.*, vol. 107, no. A12, pp. 1–16, 2002.

[21] A. Rossi, A. Cordelli, P. Farinella, L. Anselmo, and C. Pardini, "Modelling the evolution of the space debris population," *Adv. Sp. Res.*, vol. 19, no. 2, pp. 331–340, 1998.

[22] G. W. Wetherill, "Collisions in the asteroid belt," *J. Geophys. Res.*, vol. 72, p. 2429, 1967.

[23] R. Greenberg, "Orbital interactions - A new geometrical formalism," *Astron. J.*, vol. 87, no. 1, p. 184, 1982.

[24] W. F. Bottke and R. Greenberg, "Asteroidal collision probabilities," *October*, vol. 20, no. 10, pp. 879–881, 1993.